

https://dspace.org/

A novel method to measure residual stresses in unidirectional GFRP.

Reid, R.G.; Paskaramoorthy, R.

2009-05
Elsevier
http://hdl.handle.net/10539/21463
Reid, R. G. and Paskaramoorthy, R. 2009. A novel method to measure residual stresses in unidirectional GFRP. Composite Structures 88(3), pp. 388-393. DOI: 10.1016/j.compstruct.2008.04.015

Downloaded from a DSpace repository. https://dspace.org/

A novel method to measure residual stresses in unidirectional GFRP

R. G. Reid* **and R. Paskaramoorthy**

RP/Composites Facility, School of Mechanical, Industrial and Aeronautical Engineering,

University of the Witwatersrand, Johannesburg, Private Bag 3, Wits 2050, South Africa.

Abstract

A few methods are available for measuring the residual stresses that occur in the simplest of all possible composites structures – the unconstrained unidirectional laminate. None of them, however, are suitable for use on GFRP. A new method is presented whereby the stresses in a unidirectional GFRP laminate can be determined. The method relies on releasing the constraints between fibre and resin through an annealing process. The strain in the glass fibres is thus obtained, which allows the elastic stresses within the fibres and the resin to be determined. In this way, it is not necessary to take account of plasticity and viscous effects in the polymer in order to determine the stresses within the laminate. Results for unidirectional laminates initially manufactured to contain differing residual stresses are presented and discussed.

Keywords: Residual Stress; GFRP; Experimental Techniques

* Corresponding author. Tel.:+27-11-717-7309; fax: +27-11-717-7049. *E-mail address*: robert.reid@wits.ac.za

1. Introduction

Glass Fibre Reinforced Plastic (GFRP) is used very extensively in the process plant environment. Although it has excellent corrosion resistance it is susceptible to environmentally assisted cracking. The crack growth rate is significantly affected by the level of tensile stress and hence design codes frequently call for the use of safety factors in excess of 10 when dealing with structures which are to be exposed to acid [1]. The overall state of stress is affected both by mechanical loading and residual stresses. The magnitude of the residual stresses is typically small, but the use of large safety factors means that the stresses caused by mechanical loading can be comparable. Neglecting residual stresses consequently misrepresents the overall state of stress within the structure and hence the rate of crack growth. It is therefore necessary that the residual stresses be estimated.

Residual stresses within a composite structure can develop at a range of size scales. At the macro or structural scale, one part of a structure can act against another as a result of external constraints. At the meso or ply scale, internal stresses can develop due to mismatches in coefficients of thermal expansion between laminate plies, even simply from changes in fibre orientation. At the micro scale, differences in coefficients of thermal expansion between the fibres and the matrix result in internal stresses. Cure shrinkage of polymer resin systems can result in additional stresses at this scale. The overall state of residual stress in a laminated structure results from the combination of these effects and it is therefore necessary that techniques are available to measure the residual stresses at all three scales.

The state of stress at the larger scales is routinely measured by a variety of methods. Typically these approaches involve relaxing the local constraint by judicious removal of material in the

form of holes [2,3], slits [4,5] and layers [4-12] and measuring the response of the structure. The measurement techniques employed vary from strain gauging [2-4,7,8] to moiré interferometry [5,11,12] and microscopy [5,10].

These methods are not, however, really practical for measuring residual stresses within a single uniform ply of unconstrained material. The residual stresses here arise from a lack of homogeneity at the scale of the fibre diameter, typically 10-25 μm for glass fibre. The measurement systems, however, operate at a larger scale – even if just in terms of material removal. The material consequently appears uniform at the scale of the measurement systems and no stresses are measured. It is therefore necessary that some other measurement technique be utilised.

One approach is to directly measure the strain within the intramolecular bonds of the ply using Raman spectroscopy [13,14] or neutron [15] and X-ray [15,16] diffraction techniques. These approaches require that either the fibre or resin system has a crystal structure. Neither constituent of GFRP satisfies this criterion.

An alternative approach that can be used, at least for directional reinforcement, is to remove the constraint between fibre and matrix over a large fibre length. The resulting displacement of the fibre ends is significant and can be readily measured. Although this approach only allows stress in the fibre direction to be measured, the other stresses are minor in comparison. This approach has been used for measuring the axial stresses in silicon-carbide reinforced titanium [5,16,17]. Removal of the fibre constraints is achieved by etching the titanium matrix away. The matrix etching technique is not really suitable for GFRP, however, because the

fibre diameters are small. The measured change in fibre length is consequently affected by curvature enabled by the low bending stiffness of the fibres.

To the authors' knowledge, no technique has been documented that allows for the measurement of residual stress in an unconstrained ply of unidirectional GFRP. Given the importance of this material in industry and the contribution of residual stresses to one of its primary failure modes it is surprising that more attention has not been directed to this problem in the literature. This work presents a method to address this deficiency by enabling measurement of stresses in the fibre direction. The method releases the residual strains over the entire laminate simultaneously through the use of an annealing process that gradually heats the polymer matrix until its modulus decreases to negligible values. At this point, it is unable to apply significant restraint to the glass fibres. Any further heating then elicits essentially the same temperature response as that of pure glass fibre. By aligning the high-temperature response of the unidirectional laminate with that of pure glass, it becomes possible to compare the strains in the glass of the laminate to the strains expected in unloaded glass fibres at any temperature. The stresses in the glass and resin can thus be easily determined from the linear elastic response of the glass fibres. It is not necessary, therefore, to take account of plasticity and viscous effects in the polymer in order to determine the stresses within the laminate.

2. Basis of technique

When a thermoset resin system is heated past its glass transition temperature (T_g), the modulus drops until it becomes negligible. Figure 1 shows this effect for Derakane

Momentum 411-350 vinyl-ester resin, where it can be seen that at the T_g of 120°C the modulus is only approximately 2.5% of that at ambient conditions. At higher temperatures the modulus reduces still further to well below 1% of the room temperature value.

A plot of the thermal expansion of a unidirectional GFRP specimen against temperature exhibits therefore, two regions of linearity. At temperatures far below the T_g of the polymer matrix, the specimen expands at a rate between the individual rates of glass fibre and the resin system. At temperatures above the T_g of the polymer matrix, the low modulus of the resin system prevents it from affecting the thermal expansion of the glass fibres and the specimen expands at a rate equal to that of the glass alone. It is this effect that allows an absolute measure of the state of residual stress in a unidirectional GFRP specimen.

The coefficient of thermal expansion of E-glass is fairly constant, and as such the thermal expansion of the specimen is linear at temperatures above the T_g of the resin. It is thus easy to extend the measured strain back to lower temperatures, defining a locus of zero stress in the glass fibres. The difference, at any temperature, between the measured strain and the strain on the locus of zero stress defines the mechanical strain in the glass fibre. Since the modulus of glass fibre is constant over the range of temperatures required to significantly affect a polymer matrix, the stress in the glass fibres can be found at any temperature using Hooke's Law:

$$\sigma_f = E_f \varepsilon_f \tag{1}$$

where E_f and ε_f are the tensile modulus and the mechanical strain of the fibre respectively. The stress in the resin system can then be found from the relationship:

$$\sigma_r = \sigma_f \frac{V_f}{V_r} \tag{2}$$

where V_f and V_r are the volume fractions of the fibre and resin system respectively.

An important advantage of this method is that it depends only on the elasticity of the glass fibre for the determination of internal stresses. At no stage are the mechanical properties of the resin system required. It is acknowledged that heating can cause a number of highly non-linear processes to develop in the resin system. These include additional polymerisation shrinkage, viscous and plastic flow. None, however, affects the expansion of the specimen at temperatures above the T_g since the modulus of the polymer is sufficiently low that it is unable to influence the expansion of the glass fibre. As a consequence, the apparent locus of zero stress in the glass fibres is unaffected. The absolute value of the residual strain in the glass fibres can thus be determined for temperatures less than those where these processes might start developing.

3. Experimental method

Although the underlying concept of the technique is simple, performing the necessary experiments requires some care due to complications arising from the loss of resin stiffness at high temperatures. It is, for instance, not possible to make use of strain gauges for this work because the inherent stiffness of the gauges affects the strain in the underlying specimen when the modulus of the resin system decreases. It was decided, therefore, to use a displacement transducer to measure the change in specimen length and hence infer the strain. This approach meant that a reasonable specimen length was required to enable a measurable response. A consequence of this requirement is that the specimens must be symmetric to prevent measurement errors caused by thermally induced curvature.

3.1. Specimens

Two GFRP plates of 3 mm thickness and 40% nominal fibre volume fraction were produced by aligning unidirectional E-glass rovings of 400 tex between two ground steel plates and infusing Derakane Momentum 411-350 vinyl-ester resin using vacuum assistance. The fibres of one plate, designated "Unloaded", were tensioned just enough to prevent displacement of the fibres during resin infusion. The fibres of the other plate, designated "Preloaded" were pre-tensioned prior to resin infusion. The two plates were cured at a temperature of 60°C and a pressure of 6 bar. The plates were then post-cured overnight at a temperature of 92°C after which they were cooled before the preload tension was released.

The curing process allowed significant residual stresses to develop on cooling of the resin. The use of a high curing pressure ensured a laminate of nearly zero void content. The resulting plates were of very uniform thickness, with good fibre alignment.

Two sets of specimens were then cut from the plates using a rotary diamond cutter. The specimens had a length of 250 mm aligned with the fibres, a width of 20 mm and a thickness of 3 mm. Each specimen was then cut in half, "folded" double and bonded together using the same resin used for the matrix. This process ensured that symmetrical specimens were produced. Due to the flatness of the original GFRP plates, the bond layer was very thin. It was thus assumed that the bond-line did not substantially affect the fibre volume fraction of the resulting specimen of 6 mm thickness.

3.2. Equipment

Measurement of thermal expansion was accomplished by means of a dilatometer built around a Kaman Measuring Systems 1UEP non-contact displacement sensor coupled with a KD2300 oscillator/demodulator. The specimens were positioned within a steel frame and clamped in place using “blunt” knife edge grips. Similar grips were used to support a copper target over the other end of the specimen. The displacement sensor was mounted in the steel frame aiming towards the copper target. The relative change in gap width between the copper target and the displacement sensor provided a measure of the change in specimen length and hence the thermal strain.

Control of the specimen temperature was achieved by placing the entire dilatometer assembly within an oven equipped with a fan to circulate the internal air. Temperature within the oven was controlled using a JUMO dTRON 04.1 programmable temperature controller with a ramping function linked to a Pt100 temperature sensor. Temperature was measured using a LM35 integrated-circuit temperature sensor.

Output from the displacement and temperature sensors was converted to digital form using a two-channel ADC 100 data-logger from Pico Technology Limited. Data were recorded every minute, with voltages from each of the two channels being averaged over this period.

3.3. Procedure

The specimen was clamped within the dilatometer assembly. Spacers were used during this procedure to ensure that the target was positioned at a repeatable distance from the sensor.

The dilatometer assembly was positioned within the oven in such a way that the specimen was suspended vertically. This approach prevented erroneous readings resulting from lateral displacement of the specimens.

Once the data logging software was running correctly, the temperature within the oven was ramped from ambient conditions through to 140°C at a rate of 6°C per hour. The slow rate of heating was selected to accommodate two processes that can affect the accuracy of the measured results. The first process is thermal lag resulting in temperature variations within both the specimen and the test rig. The second process that must be accommodated is that of viscous flow at high temperatures. A slow heat up rate provides sufficient time to allow for viscous flow and also minimises temperature variations. By interrupting the rate of temperature increase and holding the temperature at constant values it was possible to determine if the selected ramping rate was suitable. The measured displacement did not vary significantly with time at either low or high temperatures. It was thus ascertained that the selected ramping rate was sufficiently slow.

Once the temperature had reached the maximum value the oven was turned off and the recorded results processed.

3.4. Calibration

The variation in gap width between the sensor and its target was a function of the thermal expansion of the steel dilatometer frame, the copper target and the sensor. In addition, the output voltage of the sensor varied as a function of temperature even for a fixed gap width. It was thus necessary to calibrate the sensor within the dilatometer assembly. This was accomplished by measuring the voltage output from the sensor for four reference materials. Commercially pure aluminium (1100), commercially pure copper (C10200), steel (AISI 4340) and isomoulded graphite (Ellor +20) were selected to span the expected thermal response of the specimens. Each of the specimens was tested a minimum of three times. The specimens were removed from the grips and remounted between tests. The output voltage was assumed to be a quadratic function in terms of both specimen strain and oven temperature. A least squares analysis was used to determine the calibration constants. A comparison between the known thermal response and that measured using the reference specimens indicates a very good correlation. This is shown in Figure 2.

4. Results and discussion

The measured response for the two sets of specimens is presented in Figure 3. The data have been offset to indicate a zero response at the reference temperature of 25°C. It can be seen that both sets exhibit regions of linearity at low temperatures and again at temperatures greater than about 115°C. The apparent coefficients of thermal expansion for temperatures greater than 115°C fall within the range 4.1 με/°C to 6.1 με/°C and thus agree fairly well with

the range 4.7 με/°C – 5.4 με/°C quoted for E-glass fibres [18-20]. This behaviour is exactly as predicted, validating the underlying basis for the technique.

At low temperatures the response of the two specimens sets is similar. The measured coefficients of thermal expansion fall in the range 9.1 με/°C to 10.7 με/°C. This is in good agreement with complementary strain gauge measurements, performed according to the method of Jeronimidis and Parkyn [6], which gave measurements in the range 9.3 με/°C to 10.3 με/°C.

The onset of non-linear behaviour in the unloaded specimens begins at approximately 92°C which corresponds with the post-cure temperature. Between 92°C and 115°C the unloaded specimens behave non-linearly but continue to expand with temperature. In contrast, the preloaded specimens display significant non-linearity between 65°C and 115°C to the extent that they appear to have a negative coefficient of thermal expansion between 90°C and 100°C. The difference between the non-linear behaviour of the two specimen sets is explained later in this work. It is apparent at this stage however, that the internal stress states are dissimilar and that their relaxation results in different non-linear responses.

The magnitude of the internal stresses can be readily obtained by extrapolating the linear data from high temperatures to lower temperatures as shown in Figure 4. For illustration purposes, the response of a preloaded specimen is considered. The extrapolated line defines the locus of zero stress in the glass fibres. Differences between the measured data and this locus hence define the residual strain in the glass fibres at any temperature.

The residual strains thus obtained for all specimens are shown in Figure 5. It can be seen that the preloaded specimens are essentially unstressed under ambient conditions. As the temperature rises however, the differences in thermal expansion between the fibre and resin start to affect the internal stresses. The fibres become progressively loaded in tension and the resin system is correspondingly loaded in compression. In contrast, the unloaded specimens experience their maximum state of stress at room temperature, where the fibres are in a state of compression. As the temperature rises, the differences in thermal expansion between the fibre and resin cause the internal stresses to reduce with temperature up to approximately 75°C.

The results presented in Figure 5 require further examination. Even though the strain response of the unloaded specimens is fairly linear up to a temperature of 90°C, a slow reduction in slope can be observed. This can be ascribed to the gradual reduction in resin modulus in this temperature range which is visible in Figure 1. At higher temperatures, the resin modulus decreases rapidly as shown in the same figure which allows the relaxation of internal stresses. The measured strain consequently decreases, aided also by additional polymerisation shrinkage of the resin system at temperatures greater than the post-cure temperature of 92°C.

The preloaded specimens display a similar reduction in slope at low temperatures. Again, this can be ascribed to the gradual reduction in resin modulus. At higher temperatures however, significant non-linearity is observed. The onset of this behaviour occurs at a temperature of 65°C which is well below the temperature of 95°C when the resin modulus begins to decrease rapidly. This implies that stress relaxation in the fibre is occurring through viscous flow of the resin which is later aided by rapid loss of resin modulus.

Viscous flow in the resin requires that it be subjected to both stress and temperature simultaneously. The internal stresses of the preloaded specimens increase with temperature until the onset of viscous flow becomes apparent at 65°C. The degree of viscous flow increases still further with increasing temperature. The unloaded specimens, in contrast, do not display the effects of viscous flow. This is because the internal stresses reduce with temperature. The driver for viscous flow thus gets weaker with increasing temperature up to approximately 75°C. Above this temperature, the stress increases but is still low enough that viscous flow is inhibited. Relaxation eventually occurs when the elastic modulus of the resin decreases substantially.

At this stage it is worth discussing a potential source of experimental error. It can be seen in Figure 3 that the slopes of the unloaded specimens are slightly steeper than those of the preloaded specimens at temperatures greater than 115°C even though they must display the same slope. This error arises because it is difficult to accurately measure the specimen strain at high temperatures due to the low modulus of the resin system. The calculated strain in the fibres depends entirely on this slope however, and so measurement errors are carried back into the calculations for residual strain in the glass fibre. This becomes apparent in Figure 5 where the slope of the preloaded specimens is significantly greater than that of the unloaded specimens at temperatures less than 65°C. The strain data of Figure 3, however, shows that the slopes of the two data sets are approximately equal at these temperatures and hence the slopes in Figure 5 are required also to be similar in this region.

The most satisfactory method of accommodating this is to use published data for the slope of the strain curve at high temperatures. Since the apparent slope of the measured data should correspond with the coefficient of thermal expansion for E-glass fibre, a value of 5.0 με/°C

[18], corresponding to the approximate mid-range of published data [18-20], was selected for further calculations. The results of this approach are presented in Figure 6.

It can be seen that the slopes of the two sets of data are now far more similar. Differences in slope from specimen to specimen can be traced to differences in slope in the original strain measurements presented in Figure 3. These resulted primarily from the slight variability in fibre volume fraction.

It is apparent from Figure 6 that the glass fibres of the unloaded specimens are in a small state of tension at the post-cure temperature of 92°C. This contradicts the frequent assumption that the internal stresses of unconstrained specimens are zero at the post-cure temperature [21,22]. The discrepancy arises because the specimen was not perfectly unconstrained during cure. The glass fibres were slightly tensioned around a substantial steel frame to prevent their displacement during infusion of the resin at room temperature. During heating of the GFRP specimens to the post-cure temperature, the steel frame also got heated. The frame expanded more than the fibres, straining them in the process. The expected effects of this loading on the results in Figure 6 can be calculated by evaluating the strain applied to the fibres by the frame. The fibres were strained by an amount equal to:

$$\varepsilon_0 = (\alpha_s - \alpha_f) \cdot \Delta T \tag{3}$$

where α_s and α_f correspond to the coefficients of thermal expansion of the steel and the glass fibres respectively and ΔT is the change in temperature. Taking the coefficients of thermal expansion for the steel and glass fibre as 12.0 με/°C and 5.0 με/°C respectively, and the change in temperature as 70 °C, equation (3) predicts that the glass fibres were tensioned to approximately 490 με. After the preload tension was released at room temperature, the GFRP assumed a state of internal equilibrium. A large percentage of the strain in the fibres was

relieved since the elastic stiffness of the fibres is considerably higher than that of the polymer matrix. The final strain in the fibres is found by considering the stiffness of the available load paths. In this case the final strain in the fibres is:

$$\varepsilon_f = \varepsilon_0 \frac{E_r V_r}{E_f V_f + E_r V_r} \tag{4}$$

where ε_0 is equal to 490με, E_r is the elastic modulus of the resin system and the remaining terms are defined in equations (1) and (2). Using a resin stiffness of 2200 MPa at 92°C, as estimated from Figure 1, a fibre stiffness of 72 GPa [18] and the nominal fibre volume fraction of 40%, equation (4) predicts a tensile strain of approximately 21 με. This value is in good agreement with that indicated in Figure 6.

Residual strains and stresses at the reference temperature of 25°C are presented in Table 1. Strains were calculated by taking a linear fit through the data presented in Figure 6. Stresses were determined using equations (1) and (2) based on the average strain in the glass fibres and using a modulus of 72 GPa and the nominal volume fraction of 40% for the glass fibres.

In order to appreciate the significance of the results presented in Table 1, it is worth evaluating them against the allowables contained within pressure vessel codes. BS4994 [23], for instance, limits tensile strains in a vessel to a maximum of 2000 με. At ambient conditions, the resin system of the unloaded specimens is subjected to an elastic stress of 10.9 MPa. Using a modulus of 3200 MPa, as estimated from Figure 1, the resin system is found to experience a tensile strain of approximately 3400 με, or 170% of that allowed by the code. Granted, the fibres are in a corresponding state of compression and are thus not susceptible to environmentally assisted cracking, but the analysis indicates that the overall state of stress is seriously misrepresented if residual stresses are neglected.

5. Conclusions

Based on the work presented above, the following conclusions can be drawn:

- A method has been presented that allows the state of residual stress in unidirectional GFRP to be estimated.

- The method is unaffected by non-linear effects in the resin system because it relies entirely on the elastic properties of the fibres.

- The measured response of the specimens to the annealing process is exactly as predicted, validating the underlying basis for the technique.

- Residual strains measured using the technique are in good agreement with those predicted by theory.

References

1. Stone MA, Schwartz IF, Chandler HD. Residual stresses associated with post-cure shrinkage in GRP tubes. Composites Science and Technology 1997;57(1):47-54.

2. Schajer GS, Yang L. Residual-stress measurement in orthotropic materials using the hole-drilling method. Experimental Mechanics 1994;34(4):324-333.

3. Sicot O, Gong XL, Cherouat A, Lu J. Determination of residual stress in composite laminates using the incremental hole-drilling method. Journal of Composite Materials 2003;37(9):831-844.

4. Ersoy N, Vardar Ö. Measurement of residual stresses in layered composites by compliance method. Journal of Composite Materials 2000;34(7):575-598.

5. Güngör S. Residual stress measurements in fibre reinforced titanium alloy composites. Acta Materialia 2002;50(8):2053-2073

6. Jeronimidis G, Parkyn AT. Residual stresses in carbon fibre-thermoplastic matrix laminates. Journal of Composite Materials 1988;22(5):401-415.

7. Chapman TJ, Gillespie JW Jr, Pipes RB, Manson J-AE, Seferis JC. Prediction of process-induced residual stresses in thermoplastic composites. Journal of Composite Materials 1990;24(6):616-643.

8. Månson J-AE, Seferis JC. Process Simulated Laminate (PSL): A methodology to internal stress characterization in advanced composite materials. Journal of Composite Materials 1992;26(3):405-431.

9. Eijpe MPIM, Powel PC. Residual stress evaluation in composites using a modified layer removal method. Composite Structures 1997;37(3/4):335-342.

10. Cowley KD, Beaumont PWR. The measurement and prediction of residual stresses in carbon-fibre/polymer composites. Composites Science and Technology 1997;57(11):1445-1455.

11. Joh D, Byun KY, Ha J. Thermal residual stresses in thick graphite/epoxy composite laminates-uniaxial approach. Experimental Mechanics 1993;33(1):70-76.

12. Gascoigne HE. Residual surface stresses in laminated cross-ply fiber-epoxy composite materials. Experimental Mechanics 1994;34(1):27-36.

13. Thomsen JS, Pyrz R. Creep of carbon/polypropylene model composites – a Raman spectroscopic investigation. Composites Science and Technology 1999;59(9):1375-1385.

14. Goutianos S, Peijs T, Galiotis C. Comparative assessment of stress transfer efficiency in tension and compression. Composites A 2002;33(10):1303-1309.

15. Rangaswamy P, Prime MB, Daymond M, Bourke MAM, Clausen B, Choo H, Jayaraman N. Comparison of residual strains measured by X-ray and neutron diffraction in a titanium (Ti–6Al–4V) matrix composite. Materials Science and Engineering A 1999;259(2):209-219.

16. Kendig KL, Soboyejo WO, Miracle DB. Measurement of residual stresses in Ti-15-3 SCS-9 continuously reinforced composites using X-ray diffraction and a matrix etching technique. Scripta Metallurgica et Materialia 1995;32(5):669-674.

17. Pickard SM, Miracle DB, Majumdar BS, Kendig KL, Rothenflue L, Coker D. An experimental study of residual fibre strains in Ti-15-3 continuous fiber composites, Acta Metallurgica et Materialia 1995;43(8):3105-3112.

18. ASM International. Engineered Materials Handbook - Desk Edition. Materials Park, Ohio: ASM International, 1995.

19. Chawla KK. Composite Materials - Science and Engineering - 2nd Edition. New York: Springer-Verlag, 1998.

20. Herakovich CT. Mechanics of Fibrous Composites. New York: Wiley, 1997.

21. Fletcher AJ, Oakeshott JL. Thermal residual microstress generation during the processing of unidirectional carbon fibre/epoxy resin composites: random fibre arrays. Composites 1994; 25(8):797-805.

22. Akkerman R, Wiersma HW, Peeters LJB. Prediction of springforward in continuous-fibre/polymer L-shaped parts. Composites A 1998; 29(11):1333-1342.

23. BS4994:1987. British standard specification for design and construction of vessels and tanks in reinforced composite materials. London: British Standards Institution, 1987.

Figure Captions

Figure 1. Modulus of Derakane Momentum 411-350 vinyl-ester resin as a function of temperature

Figure 2. Comparison between reference and calibrated measurements

Figure 3. Measured strain as a function of temperature

Figure 4. Locus of zero stress in glass fibres

Figure 5. Residual strain in glass fibre as a function of temperature

Figure 6. Residual strain in glass fibre as a function of temperature

Tables

Table 1
Residual strain and stress at 25°C

	Strain in Glass Fibres		Stress in Glass Fibres (MPa)	Stress in Resin (MPa)
	Average Strain $\times 10^6$	Standard Deviation $\times 10^6$		
Unloaded Specimens	-227	42	-16.3	10.9
Preloaded Specimens	47	38	3.4	-2.3

Figure 1.

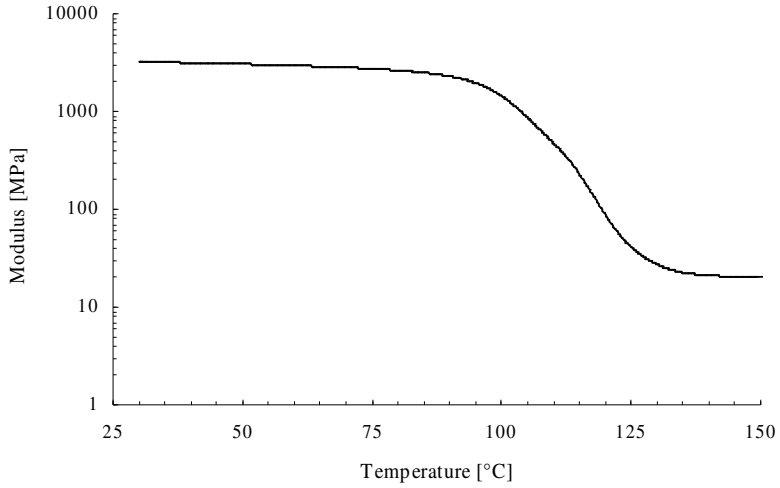
10000
1000
100
10
1
Modulus [MPa]
25
50
75
100
125
150
Temperature [°C]

Figure 2.

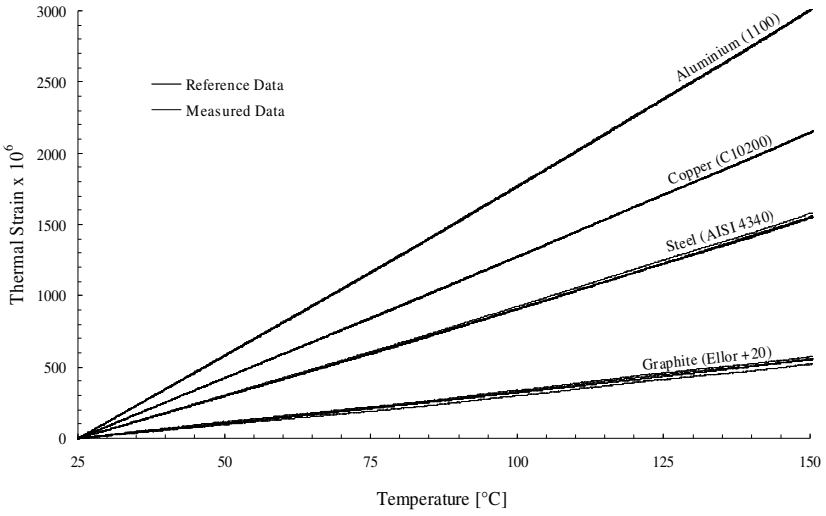
Reference Data
Measured Data
Aluminium (1100)
Copper (C10200)
Steel (AISI 4340)
Graphite (Ellor +20)
Thermal Strain x 10^6
Temperature [°C]
3000
2500
2000
1500
1000
500
0
25
50
75
100
125
150

Figure 3.

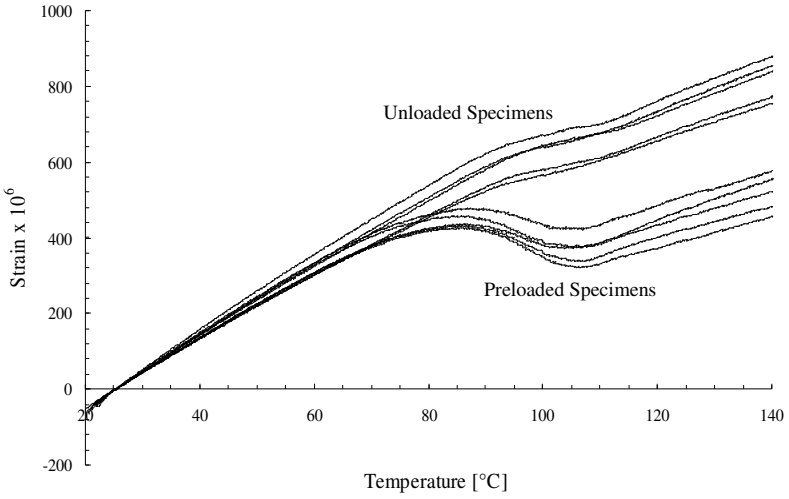
1000
800
600
400
200
0
-200
20
40
60
80
100
120
140
Strain x 10^6
Temperature [°C]
Unloaded Specimens
Preloaded Specimens

Figure 4.

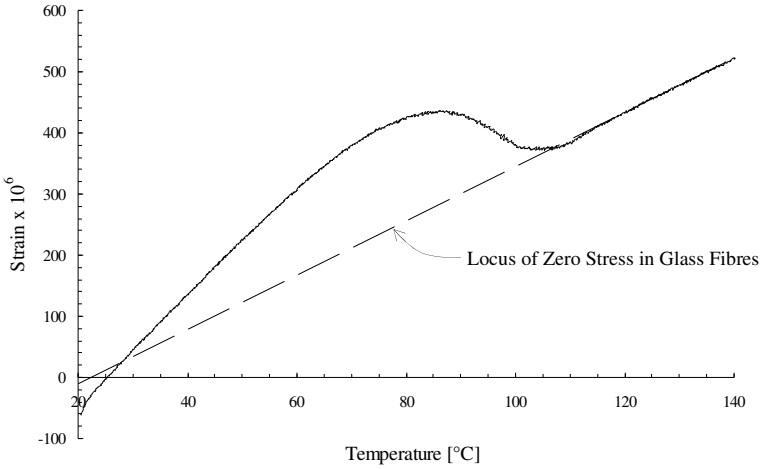
600
500
400
300
200
100
0
-100
Strain x 10^6
20
40
60
80
100
120
140
Temperature [°C]
Locus of Zero Stress in Glass Fibres

Figure 5.

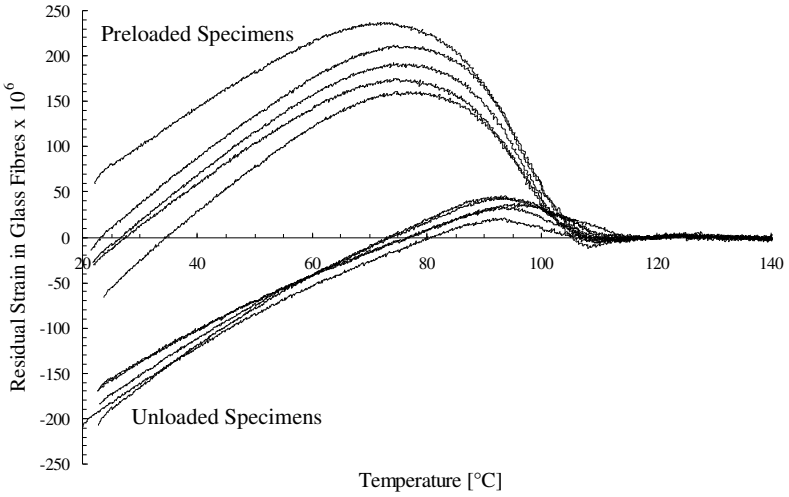
Preloaded Specimens
Unloaded Specimens
Residual Strain in Glass Fibres x 10^6
Temperature [°C]
250
200
150
100
50
0
-50
-100
-150
-200
-250
20
40
60
80
100
120
140

Figure 6.

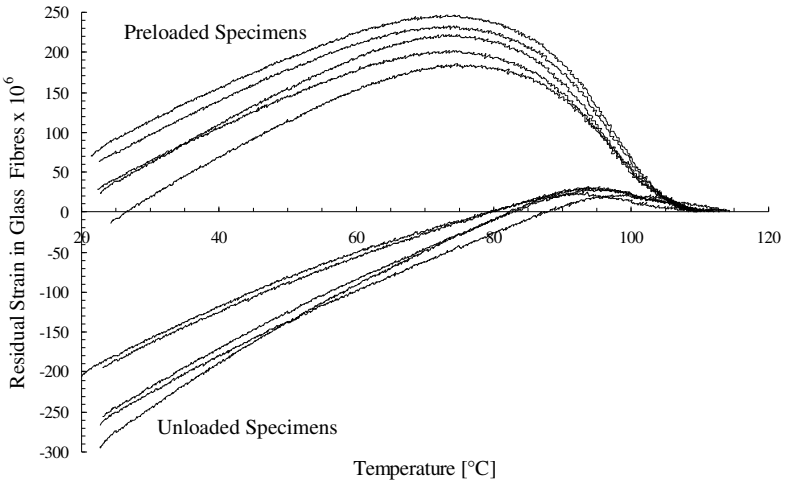
Preloaded Specimens
Unloaded Specimens
Residual Strain in Glass Fibres x 10^6
Temperature [°C]
250
200
150
100
50
0
-50
-100
-150
-200
-250
-300
20
40
60
80
100
120